Physics Letters B 769 (2017) 227–232

Contents lists available at ScienceDirect

Physics Letters B

www.elsevier.com/locate/physletb

Resonance and continuum Gamow shell model with realistic nuclear forces

Z.H. Sun, Q. Wu, Z.H. Zhao, B.S. Hu, S.J. Dai, F.R. Xu *

School of Physics, and State Key Laboratory of Nuclear Physics and Technology, Peking University, Beijing 100871, China

ARTICLE INFO

Article history:
Received 11 November 2016
Received in revised form 21 March 2017
Accepted 21 March 2017
Available online 30 March 2017
Editor: J.-P. Blaizot

Keywords:
Realistic nuclear forces
Gamow shell model
Unstable nuclei
Spectra
Resonance
Continuum

ABSTRACT

Starting from realistic nuclear forces, we have developed a core Gamow shell model which can describe resonance and continuum properties of loosely-bound or unbound nuclear systems. To describe properly resonance and continuum, the Berggren representation has been employed, which treats bound, resonant and continuum states on equal footing in a complex-momentum (complex-k) plane. To derive the model-space effective interaction based on realistic forces, the full $\hat{Q}$-box folded-diagram renormalization has been, for the first time, extended to the nondegenerate complex-k space. The CD-Bonn potential is softened by using the $V_{\text{low-}k}$ method. Choosing ^{16}O as the inert core, we have calculated sd-shell neutron-rich oxygen isotopes, giving good descriptions of both bound and resonant states. The isotopes ^{25,26}O are calculated to be resonant even in their ground states.

Resonance is a general phenomenon happening in classic or quantum systems. It plays a special role in weakly-bound or unbound quantum systems. An unbound quantum system, such as atomic cluster or unbound nucleus, can emerge in the form of intrinsic resonance. Nuclear resonances are usually followed by particle emissions as the Gamow quantum tunneling. Weakly-bound or unbound nuclei are complex open quantum systems (OQS) in which the coupling to the scattering continuum is crucial and should be properly treated. A small uncertainty in modeling would change the conclusions of physics.

In the standard shell model (SM), harmonic oscillator (HO) wave functions are always bound and localized, while a loosely-bound nucleus has small separation energy and large spatial spread, in which the continuum plays a critical role. To overcome the shortcoming of the conventional SM, the continuum shell model (CSM) [1–3] has been developed, taking into account the continuum effect by projecting the model space onto the subspaces of bound and scattering states in a real-energy basis. The continuum effect has also been well treated in the continuum coupled cluster [4] and the continuum-coupled shell model [5].

The Gamow resonance is in fact a time-dependent problem, associated with a decaying process. However, the exact treatment of the time-dependent problem is difficult. Berggren generalized the time-independent Schrödinger equation to a complex-k plane, giving single-particle (SP) bound states, unbound resonant states and nonresonant continuum states [6]. The three types of the SP states construct a complete set of basis states, called the Berggren ensemble [6]. Using the Berggren basis, the so-called Gamow shell model (GSM) has been advanced recently. With phenomenological interactions, the GSM has been successfully applied to nuclear structure calculations [7–10].

It is pursued currently to perform the first-principles calculations of nuclear structure. Such calculations require two fundamental elements: (i) using realistic nuclear forces and (ii) rigorously treating many-body correlations. The shell model which is beyond mean-field approach provides a good platform to handle many-body correlations. Starting from realistic forces, traditional core shell model [11,12] or no core shell model (NCSM) calculations [13] have obtained great success, while the GSM calculation faces big challenges. For example, the wave functions of resonant SP states are not square integrable, which complicates severely the treatments of the complex non-Hermitian Hamiltonian and other mechanical quantities. It is even more challenging to establish a GSM based on realistic nuclear forces with an inert core. In this case, one has to strive to build the model-space effective interaction in the complex-k basis. Nevertheless, the realistic core GSM (CGSM) calculation has been proposed with limit to two- or three-particle systems [14,15]. The effective interaction was built by using the degenerate $\hat{Q}$-box approach but neglecting folded diagrams

* Corresponding author.
E-mail address: frxu@pku.edu.cn (F.R. Xu).

http://dx.doi.org/10.1016/j.physletb.2017.03.054

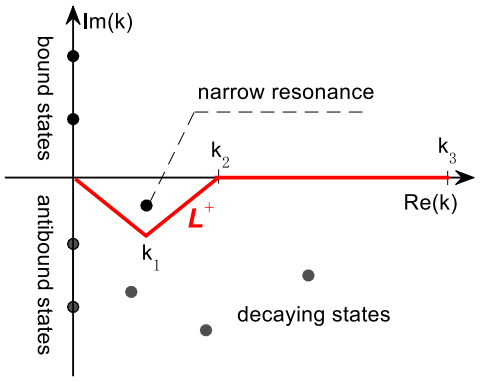

Fig. 1. Schematic Berggren complex-k plane. The scattering states lie on the L^+ contour (red line). The bound, resonant and scattering states construct the Berggren completeness relation. The contour L^+ has to be chosen in such a way that all the discrete narrow resonant states are contained in the domain between L^+ and the real k axis. (For interpretation of the references to color in this figure legend, the reader is referred to the web version of this article.)

[15]. The folded-diagram procedure is to sum up the subsets of diagrams to infinite order [12]. Recently, realistic no-core Gamow shell model (NCGSM) was developed for the light nuclei of helium isotopes [16], in which one escapes the task of building effective interaction.

In the present work, we start from realistic nuclear forces to develop a sophisticated CGSM for many-particle nuclear systems. The inert core takes a doubly magic nucleus. The realistic effective interaction in the model space is obtained by extending the non-degenerate $\hat{Q}$-box folded-diagram renormalization [17,18] to the complex-k space. With choosing ^{16}O as the inert core, we have calculated the sd-shell oxygen isotopes up to the unbound ^{26}O nucleus.

The Berggren basis is generated by the Woods–Saxon (WS) potential including spin-orbit coupling [19]. The radial wave functions of the Berggren SP states are obtained by solving the time-independent Schrödinger equation in the complex-k space,

$$\frac{d^2u(k,r)}{dr^2} = \left[\frac{l(l+1)}{r^2} + \frac{2m}{\hbar^2}U(r) - k^2\right]u(k,r), \tag{1}$$

where l is the orbital angular momentum of the nucleon motion. The momentum k and wave function $u(k,r)$ can be complex numbers (or function). $U(r)$ is the spherical WS potential generated by the core. There is no Coulomb interaction for neutrons. The piecewise perturbation method [20] has been used to solve the Berggren SP eigen equation (1). For a resonant state, the eigen energy is a complex number, $\tilde{e}_n = e_n - i\gamma_n/2$, where γ_n stands for the resonance width.

Fig. 1 shows a schematic Berggren complex-k plane. The Berggren SP states form a complete set of basis states with discrete bound states, resonant states and continuum scattering states [6]. The wave functions of resonant states are not square integrable. The exponential increase and infinitely oscillating behavior make that the resonant wave function cannot be normalized with the conventional techniques. In the present work, we use the exterior complex scaling method [21] for the normalizations of resonant states.

We use the universal WS parameters [19], but reduce the strength $|V_0|$ by 2.3 MeV to obtain a reasonable $0d_{3/2}$ resonance width compared with the experimental width extracted in ^{17}O [9]. The WS potential of the ^{16}O core gives two bound orbits $0d_{5/2}$ and $1s_{1/2}$ at energies -5.31 and -3.22 MeV, respectively, and a resonant orbit $0d_{3/2}$ with energy $\tilde{e} = 1.06 - 0.09i$ MeV. The higher orbits $f_{7/2,5/2}$, $np_{3/2,1/2}$ $(n \geq 1)$, $g_{9/2,7/2}$, $nd_{5/2,3/2}$ $(n \geq 1)$ and $ns_{1/2}$ $(n \geq 2)$ are continuum partial waves. We take the $l \leq 4$ orbits for the sd-shell calculations. The model space for the GSM calculation is $\{1s_{1/2}, 0d_{5/2}, 0d_{3/2}+d_{3/2}\text{-continuum}\}$. $0d_{3/2}$ is a narrow resonance state which plays a crucial role in the descriptions of the sd-shell nuclear resonances. In this case, the coupling between the $0d_{3/2}$ resonance and $d_{3/2}$ continuum needs to be treated carefully. Therefore, the $d_{3/2}$ continuum is included as the part of the model space in the GSM calculation. Contributions from the $0s_{1/2}0p_{3/2,1/2}$ core polarization and other continuum partial waves are taken into account by performing the $\hat{Q}$-box folded-diagram calculations. In practical computations, the continuum states on the contour L^+ need to be discretized. We use the Gauss–Legendre quadrature method [10,14,22] for the discretization.

The intrinsic A-body Hamiltonian has the following form,

$$H = \sum_{i=1}^{A}\frac{p_i^2}{2m} + \sum_{i<j}^{A} v_{ij} - \frac{\mathbf{P}^2}{2Am}, \tag{2}$$

where v_{ij} is the nucleon–nucleon interaction. p_i is the nucleon momentum in the laboratory coordinate, while $\mathbf{P} = \sum_{i=1}^{A}\mathbf{p_i}$ is the center-of-mass (CoM) momentum of the system. In shell-model calculations, usually a one-body potential U is written into the Hamiltonian, which makes calculations more convenient,

$$\begin{aligned} H &= \sum_{i=1}^{A}\left(\frac{p_i^2}{2m} + U\right) + \sum_{i<j}\left(v_{ij} - U - \frac{p_i^2}{2Am} - \frac{\mathbf{p_i}\cdot\mathbf{p_j}}{Am}\right) \\ &= H_0 + V, \end{aligned} \tag{3}$$

with $H_0 = \sum_{i=1}^{A}(\frac{p_i^2}{2m} + U)$ having a one-body form. In the present calculations, U takes the WS potential of the ^{16}O core. V is the residual two-body interaction with corrections from the CoM motion.

The Hamiltonian is intrinsic, but it is difficult to write wave functions in a relative coordinate frame. As known, it is unfeasible to antisymmetrize the wave functions of $A > 7$ systems in a relative coordinates (e.g., the Jacobi coordinates). If wave functions are expressed in the laboratory coordinates, one should consider effects from the CoM motion which can cause spurious excitations. In the standard SM with the HO basis, the CoM spuriousity can be removed by the Lawson method [23]. Unfortunately, the Lawson method cannot be used within the Berggren complex-k basis due to the fact that the $\mathbf{R^2}$ matrix elements ($\mathbf{R}$ is the CoM coordinate) cannot be regularized using the complex scaling technique. By taking the coordinates of valence particles with respect to the core CoM, the cluster-orbital shell model (COSM) can remove the CoM excitation in the GSM calculations [24,25]. In the COSM coordinates, the translation invariance is preserved. However, the transformation of the realistic force to the COSM framework is very difficult to handle, as mentioned in Ref. [10]. In the present work, we calculate low excited states with excitation energies lower than 7 MeV, while the lowest CoM excitation energy is significantly larger than 7 MeV. Therefore, we have assumed that the CoM motion is in the s-wave and its effects on low-lying states calculated with the intrinsic Hamiltonian should not be remarkable.

We derive the effective two-body interaction from the CD-Bonn potential [26] which is defined in the relative momentum space. The bare interaction has a strong short-range repulsive core which comes from the high-momentum components of the interaction. To speed up the convergences of many-body calculations, usually the bare force is softened (renormalized). We soften the CD-Bonn interaction by using the $V_{\text{low-}k}$ method [27] in which high-momentum components above a certain cutoff Λ are integrated out.

The obtained $V_{\text{low-}k}$ interaction needs to be transformed into the laboratory HO basis for shell-model calculations. This process can be done by using the Brody–Moshinsky brackets [28]. For the GSM calculations, we need to calculate two-body interaction matrix elements in the Berggren complex-k basis. The Berggren basis wave functions can be expanded in the HO states with a large enough truncation of the HO basis [14,16]. In fact, the interaction matrix elements are obtained by computing overlaps between the Berggren and HO basis wave functions. In the present calculations, for each partial wave we take $n = 0, 1, 2 \cdots 9$ HO radial nodes, which makes the maximum shell number $N_{\text{shell}} = 2n + l = 22$ with the limit of $l \leq 4$, indicating that 22 HO shells are included. We have well tested that the above HO truncation is sufficient to reach convergence.

The amplitude of the Berggren resonant wave function increases exponentially with the distance. Nevertheless, the short-range nature of the nuclear force and the Gaussian decrease of the HO wave functions lead to the good convergences of overlap computations at certain reasonably large distance. For long-range operators such as the momentum, we compute matrix elements by using the exterior complex scaling technique.

With the $V_{\text{low-}k}$ matrix elements given in the Berggren basis, we can construct the realistic effective interaction in the model space $\{1s_{1/2}, 0d_{5/2}, 0d_{3/2} + d_{3/2}\text{-continuum}\}$ for the valence neutrons outside the ^{16}O core. We have exploited for the first time the full $\hat{Q}$-box folded-diagram method to the Berggren complex-k space, to derive a realistic effective CGSM interaction that includes effects from the continuum and core polarization. The folded-diagram process is to consider high-order contributions by summing up the subsets of diagrams to infinite order [29]. In [15] where ^{25,26}O were calculated with the ^{22}O core, the neutron partial waves $s_{1/2}$, $d_{3/2}$ and $d_{5/2}$ are treated in the WS Berggren basis, while all other neutron partial waves and all proton partial waves were treated in the HO representation. In the present work, we treat all neutron and proton channels in the Berggren basis. The continuum effects are taken into account through either effective interaction or model space.

The Berggren basis contains bound, resonant and scattering states, therefore the basis states are certainly not degenerate. The usual folded-diagram approaches, such as Kuo–Krenciglowa (KK) [30] and Lee–Suzuki (LS) [31] methods which were designed for a degenerate model space, should be no longer valid for the non-degenerate Berggren space. In the present work, we exploit the so-called extended Kuo–Krenciglowa (EKK) method [17] to the complex-k space, to build the effective CGSM interaction. There is another recently developed folded-diagram method named the Z-vertex [32] which may give more stable and better convergent calculations, while the EKK method is more convenient for numerical calculations.

In practical calculations, we first calculate the $\hat{Q}$-box and its derivatives in the Berggren complex-k basis,

$$\hat{Q}(E) = PVP + PVQ\frac{1}{E - QHQ}QVP \tag{4}$$

and

$$\begin{aligned}\hat{Q}_k(E) &= \frac{1}{k!}\frac{d^k\hat{Q}(E)}{dE^k} \\ &= (-1)^k PVQ\frac{1}{(E - QHQ)^{k+1}}QVP,\end{aligned} \tag{5}$$

where k indicates the k-th derivative, and E is the starting energy. P and Q represent the model space and the excluded space, respectively, with $P + Q = 1$. Valence-linked irreducible diagrams in $\hat{Q}$-box are calculated up to the second order in perturbation. In each diagram, the intermediate SP states can be resonant, continuum or bound states.

Table 1
Calculated energies, $\tilde{E}_n = E_n - i\Gamma/2$ (in MeV), for the ground state, 2^+ and 1^+ excited states in ^{24}O, with different discretization point numbers N_L on the $d_{3/2}$ continuum contour $L^+ = \{0.0 \rightarrow (0.48 - 0.20i) \rightarrow 0.62 \rightarrow 2.2\}$ (in fm^{-1}), see Fig. 1 for the definition of the contour L^+. $\Lambda = 2.6$ fm^{-1} is used.

N_L	0^+	2^+	1^+
16	$-50.642 + 0.013i$	$-46.172 - 0.004i$	$-45.922 - 0.009i$
18	$-50.716 + 0.002i$	$-46.262 - 0.046i$	$-46.017 - 0.049i$
20	$-50.711 - 0.001i$	$-46.219 - 0.054i$	$-45.976 - 0.056i$
22	$-50.712 + 0.000i$	$-46.218 - 0.053i$	$-45.974 - 0.056i$

Different from iterating the effective interaction in the degenerate KK approach, the nondegenerate EKK method calculates the effective Hamiltonian by iterating the following equation [17]

$$\tilde{H}_{eff}^{\{n\}} = \tilde{H}_{BH}(E) + \sum_{k=1}^{\infty}\hat{Q}_k(E)\{\tilde{H}_{eff}^{\{n-1\}}\}^k, \tag{6}$$

where $\tilde{H}_{\text{eff}}^{\{n\}}$ stands for $\tilde{H}_{\text{eff}} = H_{\text{eff}} - E$ at the n-th iteration, and $\tilde{H}_{\text{BH}} = H_{\text{BH}}(E) - E$ is the Block–Horowitz Hamiltonian shifted by an energy E, with

$$H_{BH} = PHP + PHQ\frac{1}{E - QHQ}QHP. \tag{7}$$

The effective Hamiltonian is obtained by $H_{\text{eff}} = \tilde{H}_{\text{eff}} + E$, and the effective interaction is given by $V_{\text{eff}} = H_{\text{eff}} - PH_0P$. The extended $\hat{Q}$-box folded-diagram calculation provides a useful approach to include effects from the continuum and core polarization.

Here we give a summary of the model calculation. The CGSM model space is $\{1s_{1/2}, 0d_{5/2}, 0d_{3/2}+d_{3/2}\text{-continuum}\}$. The effective interaction is constructed in such a model space. Though the EKK method applies to a nondegenerate model space, it does not always give stable numerical solutions when the SM model space is very spread in energy or momentum. For this reason, the practical GSM space includes only the $0d_{3/2}$ complex-k continuum segments $(0, k_1)$ and (k_1, k_2) in Fig. 1. The continuum states near the narrow resonant state are important for the descriptions of resonant spectra. Contributions from the $d_{3/2}$ real-k continuum segment (k_2, k_3) and the $spfg$ continuum partial waves are included via the $\hat{Q}$-box folded diagrams using the extended EKK. In calculations, we take $k_2 = 0.62$ fm^{-1} (corresponding to an energy of 8 MeV) and $k_3 = 2.2$ fm^{-1} (corresponding to 100 MeV).

The non-Hermitian CGSM Hamiltonian is diagonalized in the $\{1s_{1/2}, 0d_{5/2}, 0d_{3/2}, d_{3/2}\text{-continuum}\}$ space by using the Lanczos method in the m-scheme. Due to the presence of the nonresonant continuum, the model matrix dimension increases dramatically with increasing the number of particles in the continuum. A large dimension with many particles in the continuum would be a challenge for the complex Lanczos diagonalization which selects low-lying eigenstates [10]. In the present calculations, we allow at most two valence particles in the continuum for the calculations of the oxygen isotopes investigated. We have tested that contributions from configurations with more than two particles in the continuum can be neglected, which has also been addressed in Ref. [33]. With such a truncation, the matrix dimensions of diagonalization are 422, 2989, 13509, 38705, 81490, 122447, 141513, 119701 and 77666 for $^{18-26}$O, respectively.

It is necessary to test the stabilities of numerical calculations. Table 1 gives the ^{24}O calculations obtained with different discretization point numbers (N_L). We keep 8 points on the real segment (k_2, k_3), see Fig. 1, while the point number on each

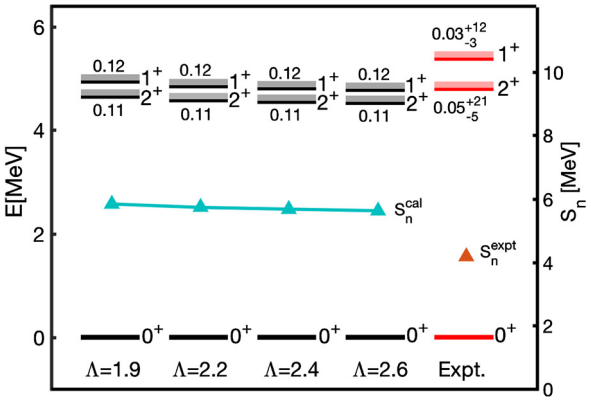

Fig. 2. Calculated excited-state spectrum for ^{24}O, at different $V_{\text{low-}k}$ cutoffs (Λ in fm^{-1}). The experimental data are from [34]. The one-neutron separation energy is also given, to see the stability of the calculations at different cutoffs.

complex-k segment $(0, k_1)$ or (k_1, k_2) varies from 4 to 7, giving the total point number from 16 to 22, see Table 1. For continuum channels without narrow resonance, we set 8 points on the real-k axis, which is found to be sufficient to provide convergence. It can be seen that $N_L = 20$ and 22 give convergent results. In following calculations, we take $N_L = 20$ and the same discretization for all the investigated oxygen isotopes with the contour $L^+ = \{0.0 \to (0.48 - 0.20i) \to 0.62 \to 2.2\}$ (in fm^{-1}). It has also been verified that the spectroscopic calculations including state resonance widths are stable against changing the contour L^+ shape. Fig. 2 shows the ^{24}O spectroscopic calculations at different $V_{\text{low-}k}$ cutoffs (Λ), showing stable results. In the figure, we also show the stability of the one-neutron separation energy against Λ. The three-nucleon force (3NF) is not considered in the present calculations. A hard cutoff with a large Λ value can reduce induced 3NFs. Therefore, we take a hard cutoff of $\Lambda = 2.6$ fm^{-1} for the calculations of the oxygen isotopes.

The ^{16}O WS Berggren basis gives an average SP energy around $e \sim -3$ MeV. Therefore, the optimal choice of the two-particle starting energy should be around $E_\omega \sim -6$ MeV. Fig. 3 displays calculated energies and resonance widths against E_ω in ^{24}O. We see that the calculations are not sensitive to the starting energy, well reproducing the excited-state spectrum and resonance widths within the experimental uncertainties [34]. The calculated ground state is bound, while the excited states are resonant. With the convergences tested above, we choose $E_\omega = -6.0$ MeV for the *sd*-shell calculations.

Neutron-rich oxygen isotopes upto beyond the neutron drip line have been investigated. Recent experiments, e.g., in Refs. [35–39], give continuing motivations to study loosely-bound or unbound oxygen isotopes. The present CGSM can well reproduce the spectra of bound oxygen isotopes. Fig. 4 displays calculations for $^{21\text{–}23}$O, compared with experimental spectra. We see that calculated spectra agree well with data. In ^{23}O, our CGSM calculation predicts that the $3/2^+$ state at $E_x = 3.5$ MeV is unstable toward neutron emission with a resonance width of 0.11 MeV, though the experiment has not observed the possible resonance.

Our interests are in loosely-bound and unbound nuclei. Fig. 5 shows the spectroscopic calculations and comparisons with existing experimental observations for $^{24\text{–}26}$O. In ^{24}O, our calculation reproduces well the experimental excited-state spectrum including observed resonance widths within the experimental uncertainties [34], while the calculations with assuming the ^{22}O core in [15] overestimate the experimental widths. ^{25}O is calculated to be resonant even in its ground state with a calculated width of $\Gamma = 0.12$ MeV that agrees with the experimental value of $\Gamma = 0.172(30)$ MeV [44] or the recent experimental datum of

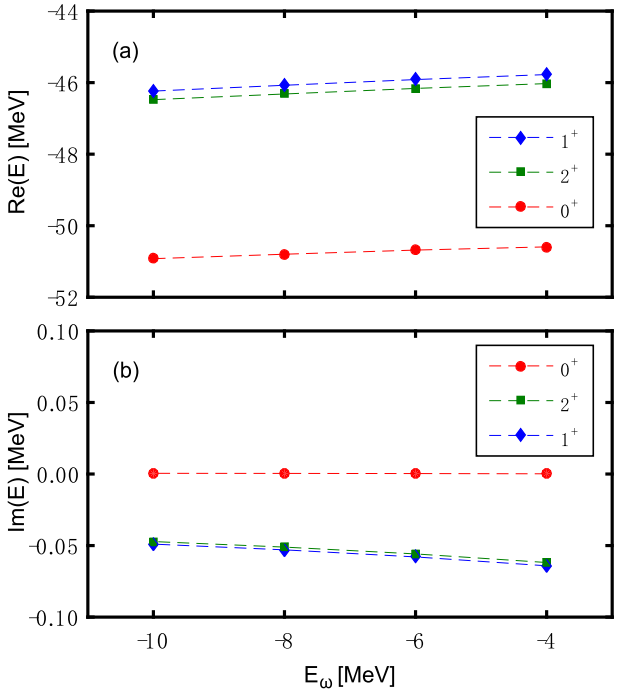

Fig. 3. Using the extended $\hat{Q}$-box folded-diagram method, the CD-Bonn CGSM (taking $\Lambda = 2.6$ fm^{-1} in $V_{\text{low-}k}$) gives stable calculations for both real (a) and imaginary (b) parts of the ^{24}O state energies against the starting energy E_ω.

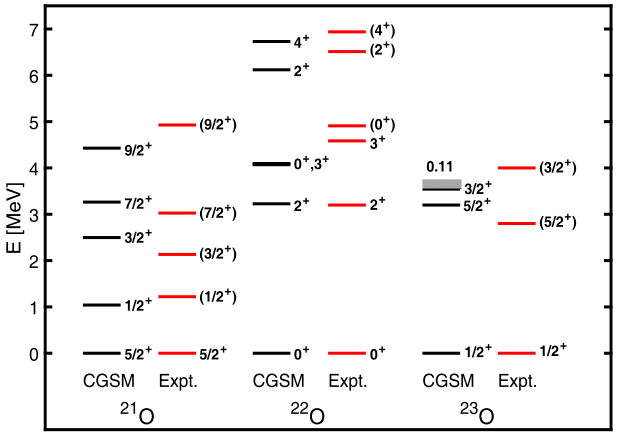

Fig. 4. Calculated spectra of ^{21,22,23}O, compared with experimental data [40–43]. The resonant state is indicated by shading, and the resonance width (in MeV) is given by the number above the level. $\Lambda = 2.6$ fm^{-1} is taken.

$\Gamma = 0.088(6)$ MeV [39]. In ^{25}O, the calculations give many broad resonant states with $J^\pi = 3/2^+$ at $E_x \gtrsim 2$ MeV, which indicates the scattering states of the $3/2^+$ channel. Due to different spins from $3/2^+$, two resonant states with $J^\pi = 1/2^+$ and $5/2^+$ at energies $E_x \approx 4 \sim 5$ MeV can be identified as our predictions in ^{25}O. The isotope ^{26}O is predicted to have a resonant ground state and two low-lying 2^+ resonant states. The recent experiment [39] did not measure resonance widths in ^{26}O, but the observed energy of a 2^+ state is consistent with our calculation. The big drop of the 2^+ state energies from ^{24}O to ^{26}O can be explained by the $N = 16$ shell. The predicted second 2^+ state in ^{26}O would correspond to the state indicated in the experiment [36].

Fig. 6 gives calculated ground-state energies and one-neutron separation energies. The WS potential reproduces well the experimental $1s_{1/2}$ and $0d_{3/2}$ SP energies, but gives the $0d_{5/2}$ energy lower than the experimental energy by 1.17 MeV. It is seen

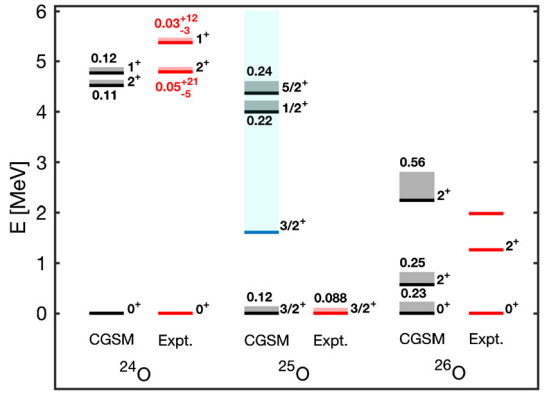

Fig. 5. Calculated spectra of ^{24,25,26}O, compared with available experimental data [34,39]. The resonant states are indicated by shading, and their widths (in MeV) are given by the numbers above or below the levels. The light blue shading indicates the scattering states of the $3/2^+$ channel. $\Lambda = 2.6$ fm^{-1} is taken. (For interpretation of the references to color in this figure legend, the reader is referred to the web version of this article.)

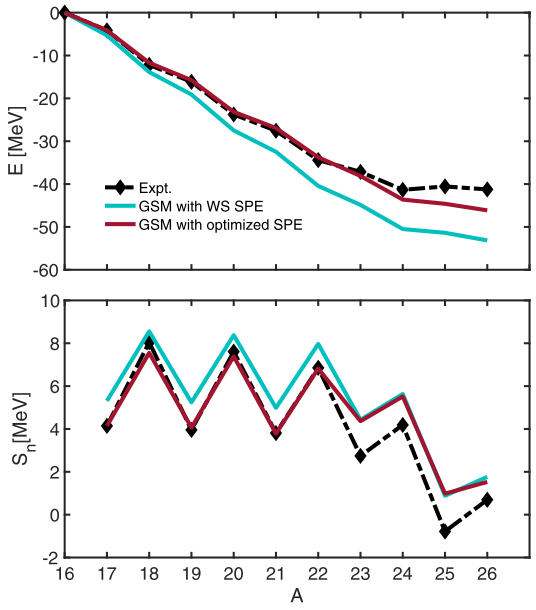

Fig. 6. Calculated ground-state energies with respect to the ^{16}O core (in upper panel) and one-neutron separation energies (in lower panel) for oxygen isotopes, compared with data [45]. "GSM with WS SPE" indicates that the calculations were done with the WS single-particle energies (SPE), while "GSM with optimized SPE" means that the calculations were done with the $0d_{5/2}$ SPE replaced by its experimental value. $\Lambda = 2.6$ fm^{-1} is taken.

that adopting the experimental $0d_{5/2}$ energy can dramatically improve the energy calculations. The deviation after ^{24}O has been addressed due to the missing of 3NFs [4,46–50].

In conclusion, we have developed a Gamow shell model with a frozen core for nuclear many-body calculations. The Berggren complex-k representation that treats bound, resonant and scattering states on equal footing has been employed. For the first time, we have extended the full $\hat{Q}$-box folded-diagram renormalization to the nondegenerate Berggren complex-k space, to construct the model-space effective interaction based on realistic nuclear forces. The continua enter into the model through either the effective interaction construction or the model space definition. The stabilities of numerical calculations have been tested. Using the $V_{\text{low-}k}$ CD-Bonn interaction and choosing the ^{16}O core, we have calculated the *sd*-shell oxygen isotopes, obtaining the good descriptions of excited-state spectra including resonance properties. The two resonant states observed in ^{24}O are well reproduced. ^{25}O is calculated to be resonant in the ground state, with the experimental width reproduced well. Resonances in the ^{26}O ground and low-lying states are predicted, providing useful information for future experiments.

Acknowledgements

This work has been supported by the National Key Basic Research Program of China under Grant No. 2013CB834402; the National Natural Science Foundation of China under Grants No. 11235001, No. 11320101004 and No. 11575007.

Appendix A. Supplementary material

Supplementary material related to this article can be found online at http://dx.doi.org/10.1016/j.physletb.2017.03.054.

References

[1] K. Bennaceur, F. Nowacki, J. Okołowicz, M. Płoszajczak, Nucl. Phys. A 651 (1999) 289.
[2] J. Rotureau, J. Okołowicz, M. Płoszajczak, Phys. Rev. Lett. 95 (2005) 042503.
[3] A. Volya, V. Zelevinsky, Phys. Rev. Lett. 94 (2005) 052501.
[4] G. Hagen, M. Hjorth-Jensen, G.R. Jansen, R. Machleidt, T. Papenbrock, Phys. Rev. Lett. 108 (2012) 242501.
[5] K. Tsukiyama, T. Otsuka, R. Fujimoto, Prog. Theor. Exp. Phys. 2015 (2015) 093D01.
[6] T. Berggren, Nucl. Phys. A 109 (1968) 265.
[7] R. Id Betan, R.J. Liotta, N. Sandulescu, T. Vertse, Phys. Rev. Lett. 89 (2002) 042501.
[8] N. Michel, W. Nazarewicz, M. Płoszajczak, K. Bennaceur, Phys. Rev. Lett. 89 (2002) 042502.
[9] N. Michel, W. Nazarewicz, M. Płoszajczak, J. Okołowicz, Phys. Rev. C 67 (2003) 054311.
[10] N. Michel, W. Nazarewicz, M. Płoszajczak, T. Vertse, J. Phys. G 36 (2009) 013101.
[11] L. Coraggio, A. Covello, A. Gargano, N. Itaco, Phys. Rev. C 80 (2009) 044311.
[12] L. Coraggio, A. Covello, A. Gargano, N. Itaco, T.T.S. Kuo, Prog. Part. Nucl. Phys. 62 (2009) 135.
[13] B.R. Barrett, P. Navrátil, J.P. Vary, Prog. Part. Nucl. Phys. 69 (2013) 131.
[14] G. Hagen, M. Hjorth-Jensen, N. Michel, Phys. Rev. C 73 (2006) 064307.
[15] K. Tsukiyama, M. Hjorth-Jensen, G. Hagen, Phys. Rev. C 80 (2009) 051301(R).
[16] G. Papadimitriou, J. Rotureau, N. Michel, M. Płoszajczak, B.R. Barrett, Phys. Rev. C 88 (2013) 044318.
[17] K. Takayanagi, Nucl. Phys. A 852 (2011) 61.
[18] N. Tsunoda, K. Takayanagi, M. Hjorth-Jensen, T. Otsuka, Phys. Rev. C 89 (2014) 024313.
[19] J. Dudek, Z. Szymański, T. Werner, Phys. Rev. C 23 (1981) 920.
[20] L.G. Ixaru, M. Rizea, T. Vertse, Comput. Phys. Commun. 85 (1995) 217.
[21] B. Gyarmati, T. Vertse, Nucl. Phys. A 160 (1971) 523.
[22] R.J. Liotta, E. Maglione, N. Sandulescu, T. Vertse, Phys. Lett. B 367 (1996) 1.
[23] R.D. Lawson, Theory of the Nuclear Shell Model, Oxford University Press, Oxford, 1980.
[24] Y. Suzuki, K. Ikeda, Phys. Rev. C 38 (1988) 410.
[25] H. Masui, K. Katō, N. Michel, M. Płoszajczak, Phys. Rev. C 89 (2014) 044317.
[26] R. Machleidt, Phys. Rev. C 63 (2001) 024001.
[27] S.K. Bogner, T.T.S. Kuo, A. Schwenk, Phys. Rep. 386 (2003) 1.
[28] M. Moshinsky, Nucl. Phys. 13 (1959) 104.
[29] T. Kuo, S. Lee, K. Ratcliff, Nucl. Phys. A 176 (1971) 65.
[30] E.M. Krenciglowa, T.T.S. Kuo, Nucl. Phys. A 235 (1974) 171.
[31] K. Suzuki, S.Y. Lee, Prog. Theor. Phys. 64 (1980) 2091.
[32] K. Suzuki, R. Okamoto, H. Kumagai, S. Fujii, Phys. Rev. C 83 (2011) 024304.
[33] N. Michel, W. Nazarewicz, M. Płoszajczak, Phys. Rev. C 70 (2004) 064313.
[34] C. Hoffman, et al., Phys. Lett. B 672 (2009) 17.
[35] K. Tshoo, et al., Phys. Rev. Lett. 109 (2012) 022501.
[36] Z. Kohley, et al., Phys. Rev. Lett. 110 (2013) 152501.
[37] C. Caesar, et al., Phys. Rev. C 88 (2013) 034313.
[38] Z. Kohley, et al., Phys. Rev. C 91 (2015) 034323.
[39] Y. Kondo, et al., Phys. Rev. Lett. 116 (2016) 102503.
[40] M.S. Basunia, Nucl. Data Sheets 127 (2015) 69.
[41] Z. Elekes, et al., Phys. Rev. Lett. 98 (2007) 102502.
[42] R.B. Firestone, Nucl. Data Sheets 127 (2015) 1.
[43] A. Schiller, et al., Phys. Rev. Lett. 99 (2007) 112501.
[44] C.R. Hoffman, et al., Phys. Rev. Lett. 100 (2008) 152502.

[45] G. Audi, F.G. Kondev, M. Wang, B. Pfeiffer, X. Sun, J. Blachot, M. MacCormick, Chin. Phys. C 36 (2012) 1157.
[46] T. Otsuka, T. Suzuki, J.D. Holt, A. Schwenk, Y. Akaishi, Phys. Rev. Lett. 105 (2010) 032501.
[47] H. Hergert, S. Binder, A. Calci, J. Langhammer, R. Roth, Phys. Rev. Lett. 110 (2013) 242501.
[48] S.K. Bogner, H. Hergert, J.D. Holt, A. Schwenk, S. Binder, A. Calci, J. Langhammer, R. Roth, Phys. Rev. Lett. 113 (2014) 142501.
[49] G.R. Jansen, J. Engel, G. Hagen, P. Navratil, A. Signoracci, Phys. Rev. Lett. 113 (2014) 142502.
[50] K. Hebeler, J. Holt, J. Menéndez, A. Schwenk, Annu. Rev. Nucl. Part. Sci. 65 (2015) 457.